

# Non-invasive Investigation of the Compartmentalization of Iron in the Human Brain

Ferdinand Schweser<sup>1,2</sup>, Jan Sedlacik<sup>3</sup>, Andreas Deistung<sup>1</sup>, and Jürgen Rainer Reichenbach<sup>1</sup>

<sup>1</sup>Medical Physics Group, Institute of Diagnostic and Interventional Radiology I, Jena University Hospital - Friedrich Schiller University Jena, Jena, Germany, <sup>2</sup>School of Medicine, Friedrich Schiller University Jena, Jena, Germany, <sup>3</sup>Neuroradiology, University Medical Center Hamburg-Eppendorf, Hamburg, Germany

**TARGET AUDIENCE** – Researchers interested in assessing the concentration and compartmentalization of brain iron *in vivo*.

**PURPOSE** – Abnormal accumulation of iron in the brain is known to be associated with several neurodegenerative diseases such as multiple sclerosis or Parkinson's disease. Hence, a major research focus currently lies on developing and applying non-invasive techniques to assess the iron concentration in the brain. Quantitative susceptibility mapping<sup>1</sup> (QSM) allows assessing the bulk tissue magnetic susceptibility which is, by its very nature, linear to the average iron concentration in the tissue.<sup>1</sup> The  $R_2^*$  relaxation rate has also recently been shown to be linear to the iron concentration<sup>2</sup>, which is remarkable, because in the presence of small inclusions  $R_2^*$  cannot be described by the static dephasing regime<sup>3</sup> and, consequently, depends in a non-linear way on the compartmentalization of the iron<sup>4</sup>.  $R_2^*$  may, in principle, change even if the total amount of iron in the tissue remains constant but the compartmentalization of the iron changes, e.g., due to the breakdown of iron-containing cells. In this contribution we show how a combination of  $R_2^*$  mapping and QSM can be used to infer on the compartmentalization of brain iron *in vivo*.

**THEORY** – The transverse relaxation rate  $R_2^*$  due to susceptibility inclusions (index "inc"), such as iron, depends on the contribution of the inclusions to the voxel magnetic susceptibility  $\chi$ , their effective size (radius  $R_{inc}$ ), and their susceptibility difference  $\Delta\chi_{inc}$  relative to the parenchyma as well as of the diffusion coefficient  $D$  in the vicinity of the inclusions<sup>4,5</sup>:  $(R_2^*)^{-1} = \chi^{-1} \cdot [405/16 \cdot D (R_{inc}/B_0)^2 (\Delta\chi_{inc})^{-1} + 9 \cdot 3^{1/2} / (2\pi\gamma B_0)]$  (1). In this context *susceptibility inclusions* are the smallest particles with a susceptibility difference seen by diffusing spins. These could, e.g., be iron-laden cells or freely dissolved aggregated iron clusters. The ratio  $\chi/R_2^* \equiv \kappa$  is independent of the total iron concentration ( $\chi$ ) in the voxel. Using  $D=2.8 \cdot 10^{-9} \text{ m}^2/\text{s}$ <sup>6</sup> yields at 3T  $\kappa = 1.10 \cdot 10^{-19} \text{ ppm} \cdot \text{s} \cdot \text{m}^2 \cdot R_{inc}^{-2} \cdot \Delta\chi_{inc}^{-1} + 3.09 \cdot 10^{-3} \text{ ppm} \cdot \text{s}$  (2). The right-most term in this Equation represents  $R_2^*$  in the static dephasing regime<sup>3</sup>. Expressing  $\Delta\chi_{inc}$  as a function of the number of iron atoms  $N_{inc}$  in the inclusion<sup>7</sup>,  $\Delta\chi_{inc} = 2.96 \cdot 10^{-26} \text{ ppm} \cdot \text{m}^3 \cdot N_{inc}/R_{inc}^3$ , shows that  $\kappa$  (in Eq. (2)) is a function of the ratio of  $R_{inc}$  and  $N_{inc}$ :  $R_{inc}/N_{inc} = (\kappa - 3.09 \cdot 10^{-3} \text{ ppm} \cdot \text{s}) / 3.72 \cdot 10^{12} \text{ ppm} \cdot \text{s} \cdot \text{m}^{-1}$  (3).  $\kappa$  may be determined, for example, by linear regression of  $\chi$  and  $R_2^*$  in regions with different iron content, e.g. in the basal ganglia.

**METHODS** – *Data Acquisition and Processing*: Double-echo gradient echo data were acquired from four healthy volunteers (male; 26-28 year old) on a 3T whole-body MRI scanner (Tim Trio, Siemens Medical Solutions, Erlangen, Germany) with the ToF-SWI-sequence<sup>8</sup>.  $R_2^*$  maps were calculated from the magnitude images using the power method<sup>9</sup> with logarithmic calculus and compensation of macroscopic field gradient contributions. Phase aliasing was resolved<sup>10</sup> and susceptibility maps were calculated from the second echo with the HEIDI algorithm<sup>11</sup>. *Evaluation*: ROIs were drawn manually in the basal ganglia nuclei using MRlcro (Version 1.39, 2005, Chris Rorden, Atlanta, GA). Rigorous least squares regression of  $R_2^*$  and susceptibility voxel values was performed for each volunteer inside the ROIs.

**RESULTS** – Figure 1 shows maps of  $R_2^*$  and magnetic susceptibility of an exemplary volunteer. Figure 2 presents the correlation of the corresponding voxel values in the basal ganglia. The average slope obtained by the linear regression in all volunteers was  $\kappa = 0.0054 \text{ ppm} \cdot \text{s}$  (range: 0.0047 to 0.0064 ppm·s;  $R > 0.6$ ,  $p < 10^{-7}$ ). Figure 3 illustrates potential configurations of iron storage,  $R_{inc}$  and  $N_{inc}$ , as a function of  $\kappa$  according to Eq. 3. The vertical black line in Fig. 3 marks the measured  $\kappa$ .

**DISCUSSION** – It has been shown that the ratio  $\kappa$  of susceptibility and  $R_2^*$  allows assessing the compartmentalization of the iron (Eq. 3 and Fig. 3). The volunteer results lead to three important implications: **First**,  $\kappa > 3.09 \cdot 10^{-3} \text{ ppm} \cdot \text{s}$  (cf. Eq. 2) shows that  $R_2^*$  due to brain iron cannot be described in the static dephasing regime, meaning that the compartmentalization of iron has a substantial effect on  $R_2^*$  and must not be neglected. **Second**, using  $N_{inc}=1000$  for H-rich ferritin<sup>12</sup> (dominant in the brain<sup>12</sup>) yields  $R_{inc}=0.62 \text{ } \mu\text{m}$  which is considerably less than the size of a single iron atom ( $R \approx 125 \text{ pm}$ ). This suggests a substantially higher number of iron atoms per inclusion, which is consistent with the histologic finding that ferritin agglomerates in oligodendrocytes<sup>14</sup>, with a radius of approximately  $2.5 \text{ } \mu\text{m}$ <sup>14</sup>. Knowing that iron occurs predominantly in oligodendrocytes (horizontal black line in Fig. 3) points to an average number of  $4 \cdot 10^9$  iron atoms per oligodendrocyte, or  $\Delta\chi_{inc}=7.6 \text{ ppm}$ . In the substantia nigra, for example,  $\chi_{inc}=0.2 \text{ ppm}$ <sup>13</sup>, leading to a relative volume fraction of oligodendrocytes of approximately 2.6%, which is in good agreement with histology<sup>14</sup>. **Third** and most interesting, the linear relation between  $R_2^*$  and susceptibility (Fig. 2) indicates that the iron loading of oligodendrocytes (reflected by  $\kappa$  through Eq. 3) is similar throughout the deep brain nuclei meaning that susceptibility and  $R_2^*$  differences are due to different volume density of oligodendrocytes, rather than due to different loading factors of ferritin or number of ferritin molecules. This conclusion relies, of course, on the assumption that the average size of the oligodendrocytes does not vary considerably throughout the different nuclei, which seems, however, reasonable.

It may be hypothesized that under pathologic conditions the iron load rather than the volume density of the oligodendrocytes changes, resulting in a decrease of  $\kappa$  according to Eq. (3), and, consequently, an increase of the number of iron atoms per cell (Fig. 3), changing the relation between susceptibility and  $R_2^*$ . Thus, a combined analysis of  $R_2^*$  and bulk magnetic susceptibility may give insights into pathologic iron deposition beyond the local changes of the iron concentration, e.g. into the breakdown of oligodendrocytes, and will be investigated in future studies. Combination of the proposed method with techniques for determining the inclusion size, e.g. combination of  $T_2$  and  $T_2^*$ , may improve the estimate of the oligodendrocyte iron load.

**CONCLUSION** – Combining  $R_2^*$  mapping and QSM allows investigating the ratio of the size and the iron load of iron-containing cells *in vivo*. The biophysical insights revealed by this approach bear the potential to be more specific to pathologic conditions than measurements of  $R_2^*$  and susceptibility alone.

**ACKNOWLEDGEMENT** – We are grateful to Christian Ziener (University of Heidelberg, Germany) and Thomas Kampf (University of Würzburg, Germany) for valuable discussions on the relaxation properties of susceptibility inclusions.

**REFERENCES** – [1] Langkammer C et al., 2012. *Neuroimage*. 59(2):1413-9. [2] Langkammer C et al., 2010. *Radiology*. 257(2):455-462. [3] Yablonskiy DA and Haacke EM, 1994. *Magn Reson Med*. 32:749-763. [4] Ziener C et al., 2005. *Magn Reson Med*. 54(3):702-6. [5] Jensen JH and Chandra R, 1999. *ISMRM*. #656. [6] Simpson JH and Carr HY, 1985. *Phys Rev*. 111(5):1201-2. [7] Schenck JF, 1992. *Ann N Y Acad Sci*. 649:285-301. [8] Deistung A et al., 2009. *J Magn Reson Imaging*. 29(6):1478-84. [9] Miller AJ and Joseph PM, 1993. *Magn Reson Imaging*. 11(7):1051-6. [10] Abdul-Rahman H et al., 2007. *Appl Opt*. 46(26):6623-35. [11] Schweser et al., 2012. *Neuroimage*. 62(3):2083-2100. [12] Harrison P and Arosio P, 1996. *BBA-Bioenergetics*. 1275(3):161-203. [13] Deistung A et al., 2012. *NeuroImage*. (epub)

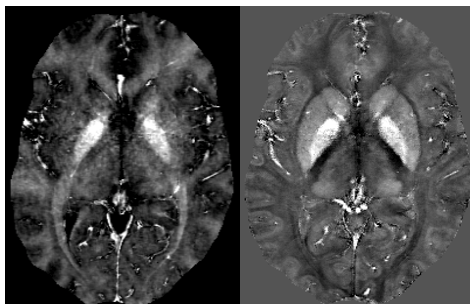


**FIGURE 1.** Exemplary maps of  $R_2^*$  (left;  $10\text{s}^{-1}$  to  $45\text{s}^{-1}$ ) and magnetic susceptibility (right;  $-0.1\text{ppm}$  to  $0.2\text{ppm}$ ) used for the analysis.

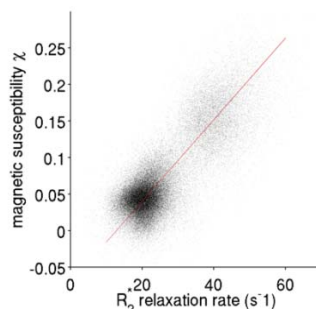


**FIGURE 2.** Correlation of  $R_2^*$  and susceptibility in the basal ganglia for the volunteer shown in Fig. 1.

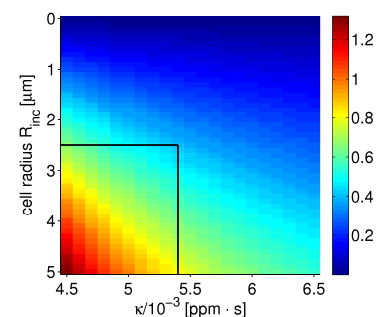


**FIGURE 3.** Number of iron atoms in iron-laden cells (divided by  $10^{10}$ ) as a function of cell size and  $\kappa$  at 3T. The intersection of the two straight lines marks the number of iron atoms ( $N_{inc}=4 \cdot 10^9$ ) in oligodendrocytes with  $R_c=2.5\text{ } \mu\text{m}$  ( $\kappa=0.0054 \text{ ppm} \cdot \text{s}$ ).